

How the Ligand Field in Lanthanide Coordination Complexes Determines Magnetic Susceptibility Anisotropy, Paramagnetic NMR Shift, and Relaxation Behavior

David Parker,* Elizaveta A. Suturina, Ilya Kuprov, and Nicholas F. Chilton



Cite This: *Acc. Chem. Res.* 2020, 53, 1520–1534



Read Online

ACCESS |



Metrics & More

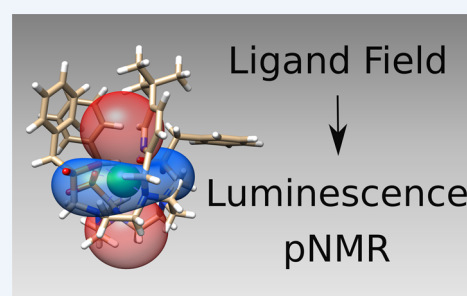


Article Recommendations

CONSPECTUS: Complexes of lanthanide(III) ions are being actively studied because of their unique ground and excited state properties and the associated optical and magnetic behavior. In particular, they are used as emissive probes in optical spectroscopy and microscopy and as contrast agents in magnetic resonance imaging (MRI). However, the design of new complexes with specific optical and magnetic properties requires a thorough understanding of the correlation between molecular structure and electric and magnetic susceptibilities, as well as their anisotropies. The traditional Judd–Ofelt–Mason theory has failed to offer useful guidelines for systematic design of emissive lanthanide optical probes. Similarly, Bleaney’s theory of magnetic anisotropy and its modifications fail to provide accurate detail that permits new paramagnetic shift reagents to be designed rather than discovered.

A key determinant of optical and magnetic behavior in f-element compounds is the ligand field, often considered as an electrostatic field at the lanthanide created by the ligands. The resulting energy level splitting is a sensitive function of several factors: the nature and polarizability of the whole ligand and its donor atoms; the geometric details of the coordination polyhedron; the presence and extent of solvent interactions; specific hydrogen bonding effects on donor atoms and the degree of supramolecular order in the system. The relative importance of these factors can vary widely for different lanthanide ions and ligands. For nuclear magnetic properties, it is both the ligand field splitting and the magnetic susceptibility tensor, notably its anisotropy, that determine paramagnetic shifts and nuclear relaxation enhancement.

We review the factors that control the ligand field in lanthanide complexes and link these to aspects of their utility in magnetic resonance and optical emission spectroscopy and imaging. We examine recent progress in this area particularly in the theory of paramagnetic chemical shift and relaxation enhancement, where some long-neglected effects of zero-field splitting, magnetic susceptibility anisotropy, and spatial distribution of lanthanide tags have been accommodated in an elegant way.



KEY REFERENCES

- Suturina, E. A.; Mason, K.; Galdes, C. F.; Kuprov, I.; Parker, D. Beyond Bleaney’s Theory: Experimental and Theoretical Analysis of Periodic Trends in Lanthanide-Induced Chemical Shift. *Angew. Chem., Int. Ed.* **2017**, 56, 12215–12218.¹ *The orientation of the main component of the magnetic susceptibility tensor differs significantly for lanthanide complexes of a common ligand; thus, one of the key assumptions in Bleaney’s theory is incorrect.*
- Vonci, M.; Mason, K.; Suturina, E. A.; Frawley, A. T.; Worswick, S. G.; Kuprov, I.; Parker, D.; McInnes, E. J.; Chilton, N. F. Rationalization of Anomalous Pseudocontact Shifts and Their Solvent Dependence in a Series of C₃-Symmetric Lanthanide Complexes. *J. Am. Chem. Soc.* **2017**, 139, 14166–14172.² *The sign and magnitude of the pseudocontact chemical shift, determined by the anisotropy of the magnetic susceptibility tensor, can be extremely sensitive to*

minimal structural changes, such as differential complex solvation.

- Harnden, A. C.; Suturina, E. A.; Batsanov, A. S.; Senanayake, P. K.; Fox, M. A.; Mason, K.; Vonci, M.; McInnes, E. J.; Chilton, N. F.; Parker, D. Unravelling the Complexities of Pseudocontact Shift Analysis in Lanthanide Coordination Complexes of Differing Symmetry. *Angew. Chem.* **2019**, 131, 10396–10400.³ *A switch in the sign of the dominant ligand field parameter and large changes in the sense, amplitude, and orientation of the main component of the magnetic susceptibility tensor may occur*

Received: May 8, 2020

Published: July 15, 2020



simultaneously and hence hide smaller NMR pseudocontact shift changes.

- Suturina, E. A.; Mason, K.; Galdes, C. F.; Chilton, N. F.; Parker, D.; Kuprov, I. Lanthanide-induced relaxation anisotropy. *Phys. Chem. Chem. Phys.* **2018**, *20*, 17676–17686. Detailed variable field proton relaxation rate analyses for isostructural series of lanthanide complexes reveal an angular dependence in both the dipolar and Curie mechanisms, demonstrated both experimentally and theoretically in a revised approach.

ELECTRONIC STRUCTURE INTRODUCTION

The unique electronic structure of trivalent 4f ions determines the distinctive properties of their coordination complexes. The electrostatic shielding of the electrons in 4f orbitals by fully occupied 5s and 5p orbitals makes the effects from surrounding ligands and other molecules far smaller than the interelectron repulsion and spin–orbit coupling (Figure 1). Due to these

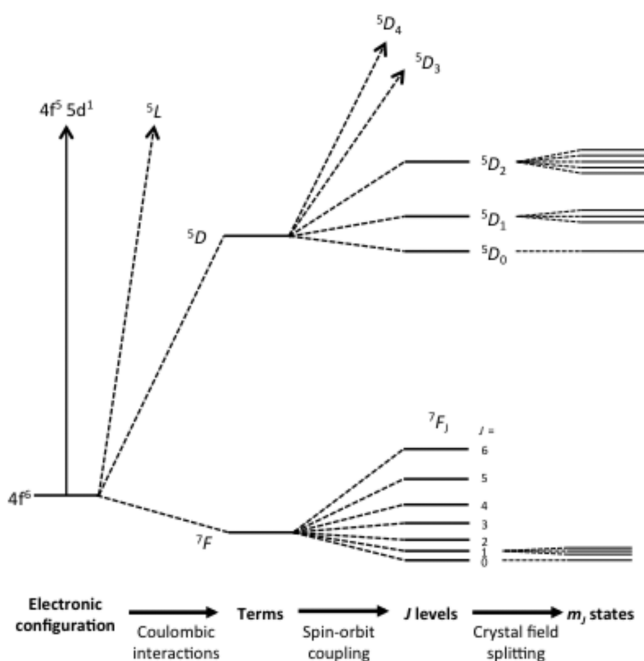


Figure 1. Schematic representation of electronic states for Eu(III) ($4f^6$): six electrons occupy seven degenerate 4f orbitals giving a 7F ground term in the Russell–Saunders coupling scheme (spectroscopic notation, $^{2S+1}L_J$), with total spin $S = 3$ and total orbital angular momentum $L = 3$. Spin–orbit coupling splits this term into seven J multiplets separated by about 10^3 cm^{-1} . Each J state is $(2J + 1)$ -fold degenerate for the free-ion; this degeneracy is partially removed upon loss of spherical symmetry. The separation of m_J states due to the ligand field is around 10^2 cm^{-1} but can be much larger.

order-of-magnitude differences, electronic transitions in lanthanide(III) complexes are often independent of the ligand environment, and the ligand field splitting can be considered on the basis of the ground-state total angular momentum, J .

The energy of m_J sublevels can be calculated using the crystal field theory that neglects mixing of f-orbitals with the orbitals of the ligands. For a given J multiplet, the model Hamiltonian has the form given in eq 1:

$$\hat{H} = \sum_{k=2,4,6} \theta_k \sum_{q=-k}^k B_q^k \hat{O}_k^q \quad (1)$$

where B_q^k are ligand field parameters, \hat{O}_k^q are Stevens operators, and θ_k are operator equivalent coefficients (Table 1), defined for

Table 1. Equivalence Coefficients for the Low-Energy Terms of Late Ln(III) Ions⁶

Ln(III)	term	θ_2	θ_4	θ_6
Eu	7F_0	0	0	0
	7F_1	$-1/5$	0	0
Tb	7F_6	$-1/99$	$2/(11 \times 1485)$	$-1/(13 \times 33 \times 2079)$
Dy	$^6H_{15/2}$	$-2/(9 \times 35)$	$-8/(11 \times 45 \times 273)$	$4/(11^2 \times 13^2 \times 3^3 \times 7)$
Ho	5I_8	$-1/(30 \times 15)$	$-1/(11 \times 10 \times 273)$	$-5/(11^2 \times 13^2 \times 3^3 \times 7)$
Er	$^4I_{15/2}$	$4/(45 \times 35)$	$2/(11 \times 15 \times 273)$	$8/(11^2 \times 13^2 \times 3^3 \times 7)$
Tm	3H_6	$1/99$	$8/(3 \times 11 \times 1485)$	$-5/(13 \times 33 \times 2079)$
Yb	$^2F_{7/2}$	$2/63$	$-2/(77 \times 15)$	$4/(13 \times 33 \times 63)$

each term and multiplet in a given configuration.^{5,6} The B_q^k parameters are defined in a particular reference frame; in symmetric molecules, the z -axis is usually aligned with the principal axes of the symmetry group, in which case the number of nonzero parameters is reduced.^{7,8} In the absence of symmetry, the expansion in eq 1 has 27 independent parameters. However, given sufficiently high symmetry or enough spectroscopic data, all nonzero ligand field parameters may be determined by luminescence spectroscopy.^{9,10} The principal parameter of interest to the NMR community is B_0^2 due to the prevalence of Bleaney's theory.¹¹ As an example, for Eu(III), it may be extracted directly from the 5D_0 to 7F_1 transition (Figure 2).^{12–14} The B_q^k parameters can be estimated from experimental data but are nowadays commonly obtained from multireference *ab initio* electronic structure methods, such as complete active space self-consistent field (CASSCF) calculations.¹⁵

Because the emissive state 5D_0 is nondegenerate, the splitting of the transition must arise from the ligand field splitting of the 7F_1 multiplet (excluding vibrational effects). Since $J = 1$, the series in eq 1 terminates at $k = 2$, and when the complex has symmetry higher than C_2 , only B_0^2 is nonzero and the spectrum exhibits two bands corresponding to the degenerate $m_J = \pm 1$ pair and the $m_J = 0$ singlet, whose separation is $\propto B_0^2$. In lower symmetry, the degeneracy of the $m_J = \pm 1$ states is lifted and $B_{\pm 2}^2$ is nonzero. Therefore, the $^5D_0 \rightarrow ^7F_1$ band can be modeled with band-specific B_0^2 and $B_{\pm 2}^2$, which may differ slightly from the parameters determined by fitting all observable bands.^{14,16} The splittings are given as $\Delta = 3\theta_2 B_0^2$ and $\delta = 2\theta_2 B_{\pm 2}^2$, and $\theta_2 = -1/5$ (Table 1), where ligand field parameters are defined for Stevens operators, and the renormalization for more commonly used spherical tensors is given in the Figure 2 caption.¹³ The sign of Δ is positive if the $m_J = 0$ component of 7F_1 is lower in energy than the barycenter of $m_J = \pm 1$ components, giving a singlet transition at higher energy than the doublet. Comparing the azaphosphinate complexes $[\text{EuL}^{8b}]$ and $[\text{EuL}^{9}]^+$ (Figure 2), there is a change in the sign of B_0^2 , which is positive for the latter. The sign of these crystal field parameters is tightly linked to the local symmetry at the Eu(III) ion.^{12,14,17,18} Even though, B_q^k parameters determined for Eu(III) complexes can be very similar to isostructural complexes of other lanthanide ions, B_q^k

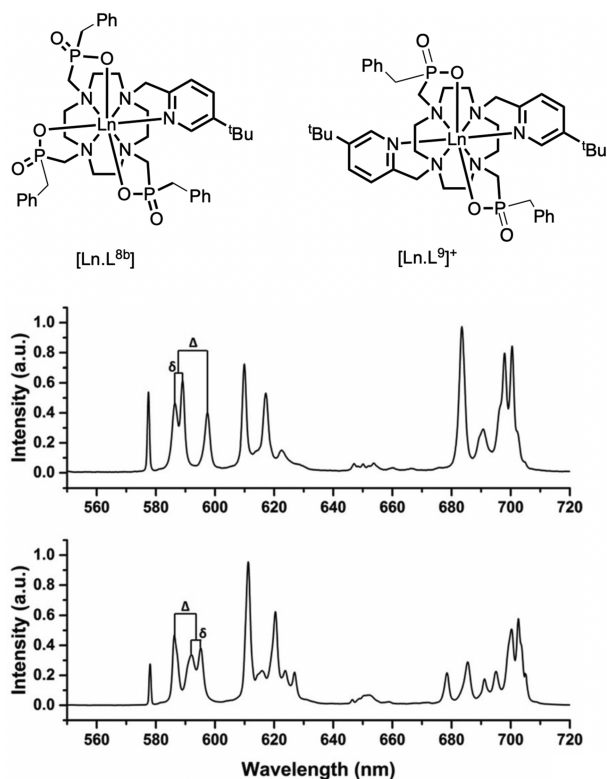


Figure 2. Europium emission spectra (295 K, MeOH, λ_{exc} 270 nm of [EuL^{8b}] (lower) and [EuL⁹]⁺ (upper) highlighting different splittings of the $\Delta J = 1$ manifold for $^5D_0 \rightarrow ^7F_1$; in the spherical operator formalism

$$\Delta = -\frac{3}{10}B_0^2, \delta = -\frac{\sqrt{6}}{5}B_2^2.{}^{15,16}$$

depends on the radial part of the f-electron wave function, which changes with nuclear charge, and small changes in bond lengths and angles may also affect the angular part of B_q^k unexpectedly.

When the ligand field splitting is comparable to the splitting between spin–orbit multiplets, J is no longer a good quantum number, and the coupling scheme breaks down, for example, for Sm(III),¹⁹ leading to the phenomenon of “ J mixing”, commonly invoked to explain unusual oscillator strengths and odd transitions in polarized emission spectra.^{20–22} Despite this, many other spectral phenomena defy explanation, and “ J mixing” is often cited as a “catch-all”, highlighting limitations in current understanding.^{12,14,23}

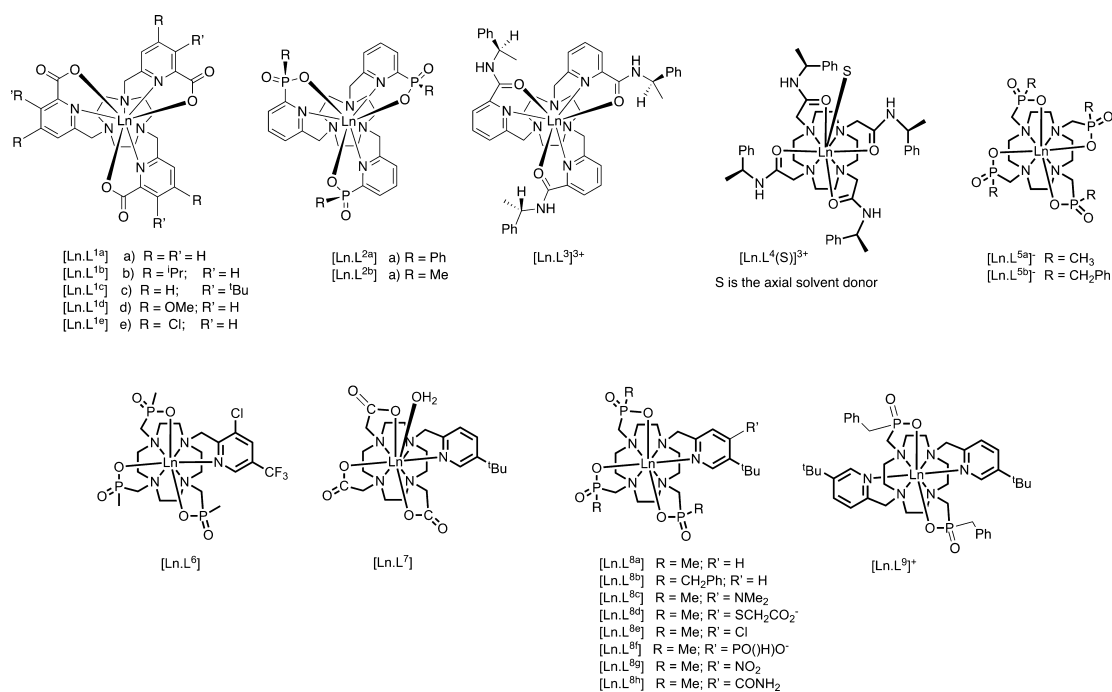
Lanthanide magnetic moments,²⁴ which are often assumed to be independent of coordination environment^{25,26} also routinely show reductions in room-temperature susceptibility values compared to the free-ion due to the ligand field effect; a notable 11% reduction was found for Ho(III).²⁷ Apart from the reduction of the average magnetic susceptibility, the ligand field also induces magnetic anisotropy that is the origin of paramagnetic NMR shifts and dramatically alters nuclear spin relaxation.

OVERVIEW OF FACTORS DETERMINING LIGAND FIELD SPLITTING

The spectral behavior of several series of macrocyclic lanthanide(III) complexes [LnL^{1–9}] has been studied, owing to their interest as emissive probes in optical spectroscopy and microscopy^{28–30} or contrast agents in magnetic resonance imaging.^{13,17,18}

Design of complexes with desired optical and magnetic properties requires an understanding of correlations between molecular structure and the electromagnetic susceptibility tensors.³¹ These correlations are often assumed to follow simple models. However, Judd–Ofelt–Mason theory fails to offer guidelines for the design of emissive lanthanide optical probes,^{32–34} and similarly Bleaney’s theory of magnetic anisotropy^{11,35,36} has been widely used for NMR spectral fitting but provides no guidance for paramagnetic shift reagent design.^{37,38}

Chart 1



Examination of the emission spectral properties of the $[\text{LnL}^{1-9}]$ series permits a dissection of the key factors determining the most important contribution to the ligand field. The size and sign of B_0^2 varies widely across these series of complexes (Chart 1 and Table 2).

Table 2. Values of Second Order Crystal Field Terms for Eu(III) Complexes^a

complex	B_0^2, cm^{-1}	B_2^2, cm^{-1}
$[\text{EuL}^{1a}]$	$<-200^d$	0
$[\text{EuL}^{2a}]$	$<+200^d$	0
$[\text{EuL}^{3}]^{3+}$	$+230^d$	0
$[\text{EuL}^4(\text{H}_2\text{O})]^{3+}$	-470^b	0
$[\text{EuL}^{5a}]^-$	-700	0
$[\text{EuL}^{5b}]^-$	-650	0
$[\text{EuL}^6]$	-550	-145
$[\text{EuL}^7]$	-455	-120
$[\text{EuL}^{8a}]$	-660	-122
$[\text{EuL}^{8b}]$	-650	-80
$[\text{EuL}^9]^+$	$+735^c$	-220^c

^aFrom emission spectra at 295 K in H_2O . Ligand field parameter values quoted in the spherical tensor formalism. ^bWith different axial donors, values changed dramatically, for example, MeCN (-630), DMF (-340), DMSO (-150), and HMPA (-85), and with fluoride replacing the coordinated water molecule, B_0^2 has a positive sign. ^cIn methanol, values were +920 and -153 cm^{-1} . ^dData recorded in methanol, not water, where values are smaller; the value for $[\text{EuL}^{2a}]$ represents an upper limit, owing to the lack of spectral resolution.

Variation of Complex Constitution and Symmetry

- In the series of C_3 -symmetric complexes, $[\text{EuL}^{1-3}]$, the triacetate, triphosphinate, and triamide ligands gave values for B_0^2 , $[\text{EuL}^2] = [\text{EuL}^1] < [\text{EuL}^3]^{3+}$. The sign is negative for $[\text{EuL}^1]$ but positive for the other two in methanol.³⁹ The polarizability of the oxygen donor atoms can be hypothesized to determine the multipolar ion–oxygen interaction energy.
- In the series of square antiprismatic complexes, $[\text{LnL}^4(\text{S})]^{3+}$, the axial donor, S, can be permuted.^{40–43} When S is MeCN, $B_0^2 = -630 \text{ cm}^{-1}$ and replacement of MeCN by a more polarizable oxygen donor is energetically favorable in the sequence: $\text{H}_2\text{O} < \text{DMF} < \text{DMSO} < \text{HMPA}$ (B_0^2 , $-470 < -340 < -150 < -85 \text{ cm}^{-1}$), correlating with the dipole moment change.⁴⁴ When the axial donor is replaced by fluoride, B_0^2 inverts sign causing a large change in magnetic susceptibility anisotropy, as the order of the m_j sublevels switches.³¹ The importance of the “axial component” of the ligand field was highlighted by Di Bari,⁴⁵ examining spectral behavior of $[\text{YbL}^5]^-$ complexes. Another example of switching sign in B_0^2 for Yb(III) complexes combined NMR, EPR, and computational studies to track changes in the anisotropy of the magnetic susceptibility tensor.⁴⁶
- For $[\text{EuL}^{1a-e}]$ (Chart 1), B_0^2 changes as the *para* substituent in the pyridine ring varies. A linear correlation between the Hammett parameter, σ_p , and B_0^2 ($R^2 = 0.97$, in acetonitrile), is consistent with the strongly dipolar nature of the Ln–N_{py} interaction.⁴⁶ The variation of overall ligand polarizability and its directionality, involving the electrostatic interaction between induced dipoles on the ligand and the quadrupole moment on the Ln³⁺ ion, is important in determining the “allowedness” of f–f

electronic transitions.^{47,48} Thus, it is the overall ligand molecular polarizability that is important in determining the ligand field.

- Other examples of switches in the sign of B_0^2 can be identified when complex constitution and local symmetry vary. The difference between the emission spectra of $[\text{EuL}^{8b}]$ and $[\text{EuL}^9]^+$ (Figure 2) is consistent with a change in sign, as symmetry changes from C_1 to C_2 .^{3,14} Other cases have been reported, including systems involving reversible coordination of a polarizable N atom, which following protonation is replaced by water.^{49–51}

Polyhedral Distortion

In point-charge ligand field theory, the geometric position and charge of each atom determine contributions to the ligand field potential. An axial anionic donor gives a positive contribution to B_0^2 , which becomes negative if it is in an equatorial position (switching at the “magic angle” $\theta \approx 54.7^\circ$ or 125.3°),^{52–55} leading to sensitivity of the ligand field potential to polyhedral distortion. The tricapped trigonal prismatic geometry is particularly sensitive, as noted by Binnemans, if all nine ligands are equivalent and the two sets of axial donors have polar angles 45° and 135° , leading to exact cancellation of all contributions and hence $B_0^2 = 0$.⁵⁶

The situation with $[\text{LnL}^{1-3}]$ is different. The first coordination sphere has three sets of donors: nitrogen atoms from the macrocycle (N_{ax}) lie in axial positions (polar angle $\theta \approx 142^\circ$); pyridyl N atoms in equatorial positions (N_{eq} , $\theta \approx 90^\circ$); carboxylate oxygens in axial sites ($\theta \approx 50^\circ$).² In $[\text{LnL}^{1a}]$, the two sets of N donors (N_{ax} , N_{eq}) give contributions to B_0^2 of similar magnitude but opposite sign and cancel out; this is because the opposite of a ligand in an axial position is a ring of donors in the equatorial plane, and here the 3-fold equatorial disposition of N_{eq} balances the N_{ax} contribution. However, the oxygen donors lie close to the magic angle, and thus the ligand field is almost entirely ascribed to the oxygen atoms, resulting in an exquisite sensitivity of ligand field and magnetic anisotropy to very small variations in their angular position (Figure 3).² Emission studies with $[\text{EuL}^{1a}]$ showed a pronounced dependence of B_0^2 on solvent, suggesting that hydrogen bonding interactions with the oxygen donors could alter their effective polar angle θ . Indeed, the X-ray structure of $[\text{YbL}^{1b}]$ shows hydrogen bonding of water to the coordinated carboxylate oxygen, demonstrating this “tugging” on the donor oxygen. For $[\text{YbL}^{1b}]$, $[\text{YbL}^{1c}]$, and $[\text{EuL}^{1e}]$, both carbonyl and carboxylate oxygen atoms served as hydrogen bond acceptors to the water hydrogen atom.⁴⁶

In 9-coordinate lanthanide complexes based on 12-N₄ (e.g., DOTA¹⁸), the most common geometries are a monocapped square antiprism (SAP) and a twisted version (TSAP). The twist angle between upper and lower planes of four donor atoms found in X-ray analyses vary around 40° and 25° , respectively. Values of B_0^2 for $[\text{EuL}^{10-15}(\text{OH}_2)]$ (Chart 2, Table 3) show larger parameters in the SAP series.^{40–44,57} These variations relate to polyhedral distortion but may also be ascribed to changes in the axial water distances that are systematically longer ($<0.3 \text{ \AA}$) in the TSAP series due to increased steric demand. Such behavior is consistent with the concept of nonintegral metal ion hydration states, reducing in value between unity (Eu) and zero (Yb), through certain TSAP series, as the bond length to the water oxygen increases.^{40–43,58}

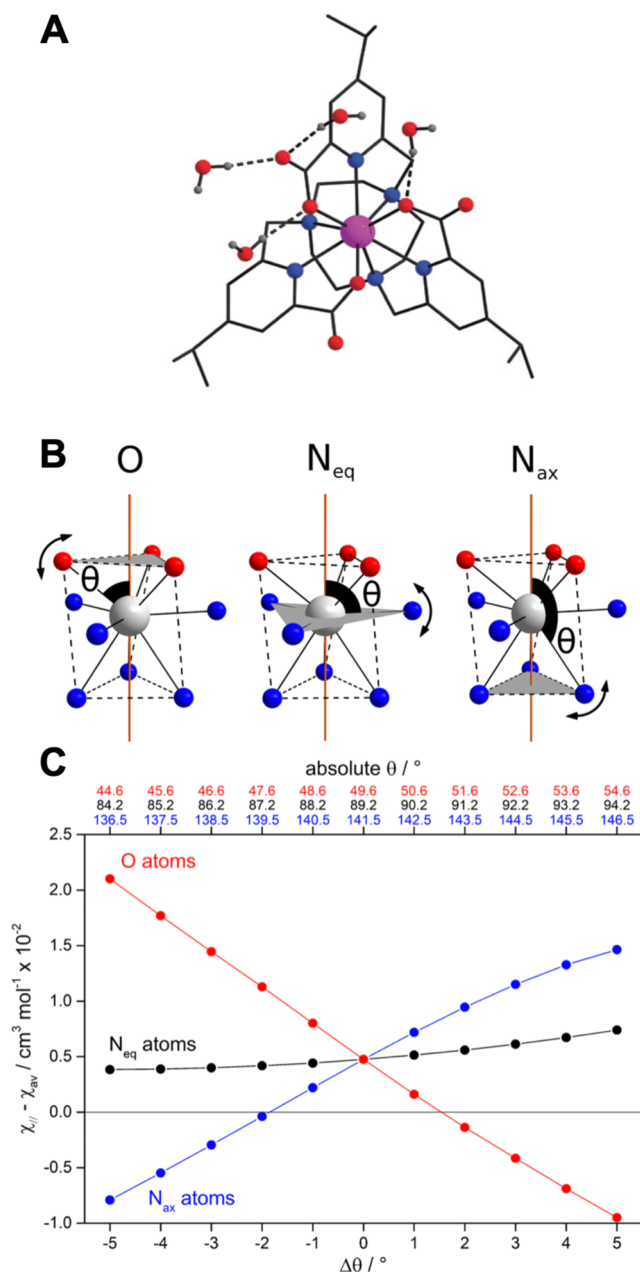


Figure 3. (A) X-ray crystal structure of [YbL^{1b}], showing hydrogen bonding of water, tugging at the ligand oxygen atoms. (B) Schematic representation of the change in the polar angles θ for the oxygen, N_{eq} (py) and N_{ax} (ring) donor atoms in [DyL^{1a}]. (C) Calculated room temperature magnetic susceptibility anisotropy arising from distortion, where $\Delta\theta$ is the deviation from the lowest energy structure.²

Supramolecular Effects: Solvation and the Degree of Aggregation

The nature of the solvent and the state of complex aggregation are supramolecular effects. For [EuL^{1b}] and [EuL^{1a}] where no solvent is bound, emission spectra change significantly with solvent, highlighted in the $\Delta J = 1$ manifold (Figure 4).⁴⁶ The variation can be attributed to differing time-averaged orientations of solvent dipoles, perturbing the Ln–O and Ln–N_{py} dipolar and quadrupolar interactions, consistent with solvent multipolar effects.^{47,48,59–61} DOSY NMR studies of the diamagnetic analogue [YL^{1b}] revealed clear evidence for aggregation that was greatest in chloroform and was positively

correlated with the ligand field splitting.⁶² With [YL^{1a}], in water only the monomer was evident, whereas in CD₃CO₂D and CF₃CO₂D, the aggregation state was 4 to 5.

In summary, ligand field splitting of lanthanide complexes is a sensitive function of several factors: the nature and polarizability of the ligand and its donors; the type and degree of polyhedral distortion; the presence and extent of solvent dipolar interactions; hydrogen bonding effects and the degree of supramolecular order. Each factor may be non-negligible in defining the ligand field, and their relative importance varies for different lanthanides.

■ PSEUDOCONTACT SHIFT AND BLEANEY'S THEORY OF MAGNETIC ANISOTROPY

When a lanthanide is treated as a point with second-rank magnetic susceptibility and infinitely fast magnetic relaxation, an additional isotropic shielding experienced by nearby nuclei is given by⁶³

$$\delta^{\text{PCS}} = \frac{1}{12\pi r^3} [\chi_{ax} (3 \cos^2 \theta - 1) + 3\chi_{rh} \sin^2 \theta \cos 2\phi] \quad (2)$$

where θ , ϕ , and r are nuclear coordinates in the eigenframe of the magnetic susceptibility tensor. The eigenvalues of the traceless susceptibility tensor are labeled to satisfy the relation $|\chi_x| < |\chi_y| < |\chi_z|$, with axiality $\chi_{ax} = 3\chi_z/2$ and rhombicity $\chi_{rh} = (\chi_x - \chi_y)/2$. Below we also use terms of $\chi_{av} = \text{Tr}(\chi)/3$ and $\chi_{\parallel} = \chi_z + \chi_{av}$.

Bleaney's theory of magnetic anisotropy^{11,35,36,64} shows that for a well-isolated J multiplet in the high temperature approximation, the anisotropy of the susceptibility tensor depends only on the second rank B_0^2 and B_2^2 ligand field parameters:

$$\chi_{ax} = -\frac{\mu_0 \mu_B^2 C_J B_0^2}{10(kT)^2}; \quad \chi_{rh} = -\frac{\mu_0 \mu_B^2 C_J B_2^2}{30(kT)^2} \quad (3)$$

where C_J is Bleaney's constant, defined for each lanthanide(III) ion ($C_J = -158$ (Tb), -181 (Dy), -71.2 (Ho), $+58.8$ (Er), $+95.3$ (Tm), and $+39.2$ (Yb)), and μ_B is the Bohr magneton.

Approximations and Their Limits

Assuming that the ligand field parameters do not vary between lanthanide ions, eq 3 suggests that χ_{ax}/χ_{rh} remains constant within the series and PCS only varies due to the change in the value of C_J . However, if the overall ligand field splitting is greater than kT (Figure 5),^{28,63,65} the Bleaney formula is no longer valid, and χ_{ax}/χ_{rh} and the eigenframe of the susceptibility tensor will depend on temperature.⁶⁶ It is evident from low temperature measurements of [LnL¹⁰](H₂O)][−] that the principal axis changes direction by up to 90° from Tb to Yb.^{67–69}

Wave function calculations accounting for orbital degeneracy and correlation among the 4f electrons, as well as spin–orbit coupling (CASSCF-SO method), are used to determine ligand field splittings in lanthanide complexes.^{70,71} Such calculations (e.g., for [LnL^{8a}], Figure 5) clearly show that in all cases the splitting is larger than kT . Thus, if eqs 2 and 3 are used to determine B_0^2 and B_2^2 from PCS data, the parameters may appear to be very different for each lanthanide simply because Bleaney's approximations do not hold.⁷²

Equation 2 also assumes a point magnetic source at the nuclear position of the lanthanide ion; a revised approach has recently emerged where the distribution of 4f electron density can be accounted for.⁷³ There are two distinct reasons for such a distribution to occur: (i) spin delocalization and (ii) fast tag

Chart 2

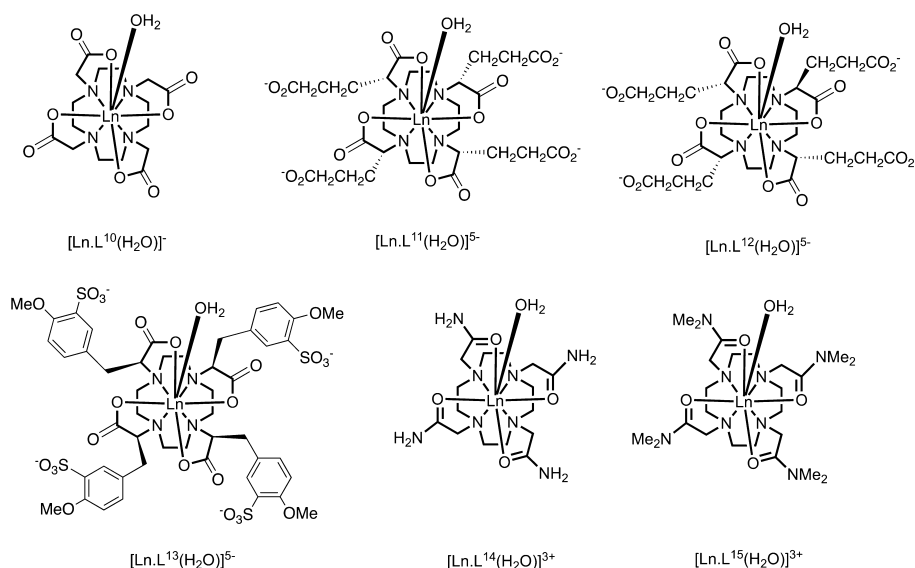


Table 3. Values of B_0^2 (Spherical Tensor Formalism) Determined by Emission Analysis for $[\text{EuL}^{10-15}(\text{OH}_2)]$

complex	B_0^2, cm^{-1}	
	SAP isomer	TSAP isomer
$[\text{EuL}^{10}]$	−630	−400
$(RRRR)-[\text{EuL}^{11}]^{5-}$	−760	−425
$(RRRS)-[\text{EuL}^{12}]^{5-}$	−780	−445
$(SSSS)-[\text{EuL}^{13}]^{5-}$	−700	−410
$[\text{EuL}^{14}]^{3+}$	−475	−205
$[\text{EuL}^{15}]^{3+}$	−450	−185

mobility. Disregarding the nature of the distribution, the mathematical formulation is the same. The effect of spin delocalization across ligands can be easily accounted for by *ab initio* calculation of the dipolar hyperfine tensors, but the tag mobility is often ignored despite the possible $\sim 30\%$ deviation from a point model for nuclei close to the tag.⁷⁴

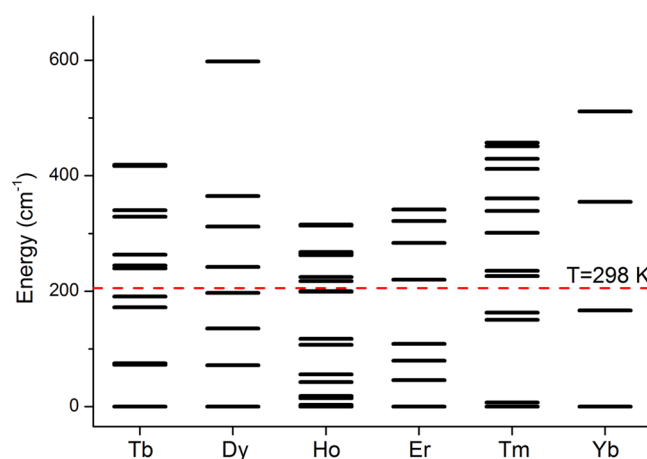


Figure 5. Energy splitting of the ground terms of $[\text{LnL}^{8a}]$ due to the ligand field, computed with CASSCF-SO in MOLCAS 8.0.¹

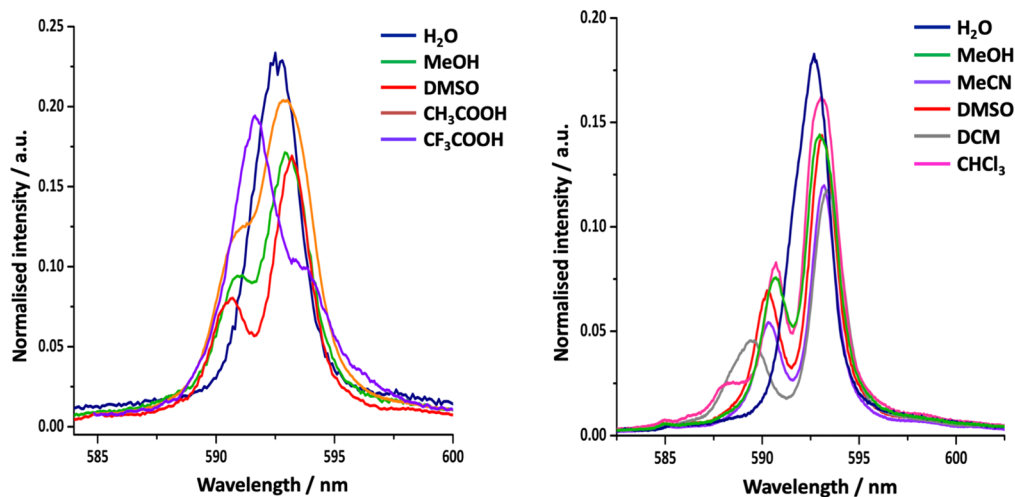


Figure 4. (left) $\Delta J = 1$ manifold for $[\text{EuL}^{1a}]$ in the stated solvents revealing the sign change of B_0^2 in $\text{CF}_3\text{CO}_2\text{H}$. (right) Related emission spectra for $[\text{EuL}^{1b}]$ in the given solvents (298 K, $\lambda_{\text{exc}} = 268 \text{ nm}$).^{46,62}

Contact Contribution to Paramagnetic Shift

In most of the cases considered in this review, the proton contact shift is negligible compared to the PCS, and the point-dipole approximation in eq 2 is valid. The contact shift is proportional to the isotropic hyperfine coupling (itself related to spin density at the nucleus) and the isotropic magnetic moment of the lanthanide ion. Accounting for admixture of excited states with different J to the ground term, the isotropic magnetic moment can be corrected,⁷⁵ and the ratio of contact contribution to the PCS can be estimated for different lanthanides provided that all other parameters in the series stay the same.⁷⁶ Such estimations suggest that in the Tb–Yb series the most pronounced effect of a contact contribution is expected for Ho/Er.

NMR SHIFT BEHAVIOR OF SYSTEMS WITH LARGE MAGNETIC ANISOTROPY

Detailed analyses of PCS data have been undertaken for isostructural complexes, with known solution speciation.^{28,38,77–81} A semiautomated combinatorial assignment procedure using PCS data, XRD structure and NMR relaxation rates to limit the combinatorial space (in Spinach⁸²) was deployed for $[\text{LnL}^{8a}]$, enabling assignment of almost every proton resonance.¹ Subsequently, the traceless part of the magnetic susceptibility tensor was obtained by fitting eq 2 to experimental data, giving excellent agreement ($R^2 > 0.99$).

The experimentally determined susceptibility tensor can be displayed as a PCS field (Figure 6), revealing significant variations in the amplitude, shape, and orientation for the $[\text{LnL}^{8a}]$ series. Bleaney's theory predicts that only the amplitude and sign should vary. However, the tensors change from almost fully rhombic (Dy and Tb; PCS field resembles d_{xz} orbital) to near axial (Tm, PCS field resembles d_{z^2} orbital). Critically the tilt angle β of the main anisotropy axis, relative to the molecular pseudosymmetry axis, varies significantly between complexes: Tb 8°; Dy 20°; Ho 22°; Er 8°; Tm 6°; Yb 23°.

To illustrate the sensitivity of magnetic susceptibility anisotropy to structural change, consider PCS shifts for $[\text{YbL}^{8b}]$ and $[\text{YbL}^{9+}]$ (Chart 3). The ¹Bu NMR chemical shifts vary markedly across the series but appear in the same order, notwithstanding the B_0^2 sign inversion (Figure 7 and Figure 2);³ Bleaney's theory predicts the shift sense should be inverted.

The explanation lies in the magnetic susceptibility tensors, expressed in their very different PCS shift fields. While the second-order magnetic anisotropy changes sign, the negative PCS lobe is still oriented in the “equatorial plane”, because along with the change in sign of B_0^2 , there is a 90° rotation in orientation of the principal magnetic axis. Thus, the combined effect of the change in sign and orientation of the ligand field were shown to give rise to similar PCS fields for the ¹Bu protons, explaining the “hidden” changes in PCS behavior.³

NMR SHIFT BEHAVIOR OF SYSTEMS WITH SMALL LIGAND FIELD SPLITTINGS

Complexes $[\text{LnL}^{1-3}]$ adopt tricapped trigonal prismatic structures and possess small ligand field splittings close to kT . Yet, their PCS values do not conform to Bleaney's theory.^{31,37,38} Both the sign and magnitude of their ligand field parameters are sensitive to local polarity changes and polyhedral distortion. They are particularly sensitive to perturbation of the polar angle of oxygen donor atoms, θ , defining the angle subtended by the Ln–O vector compared to the C_3 axis. As θ lies close to the

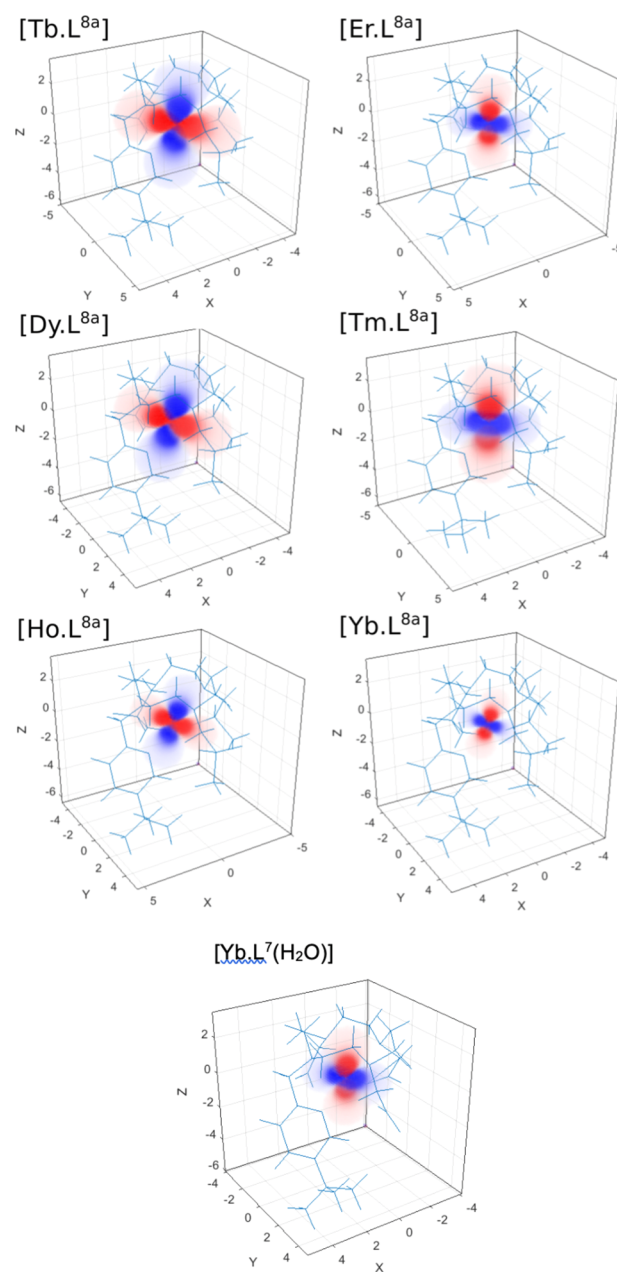
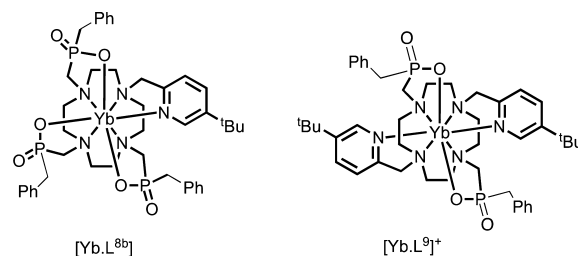


Figure 6. Pseudocontact shift fields for $[\text{LnL}^{8a}]$, reconstructed using Spinach⁸¹ with the “best-fit” magnetic susceptibility tensor. Positive PCS, red; negative, blue. Note changes in the orientation, size, and tilt of fields between $[\text{LnL}^{8a}]$ complexes¹ and how the change in coordination in $[\text{YbL}^7(\text{H}_2\text{O})]$ vs $[\text{YbL}^{8a}]$ affects the PCS field.⁸³

Chart 3



“magic” angle, small variations cause major changes in magnetic susceptibility anisotropy.^{2,46}

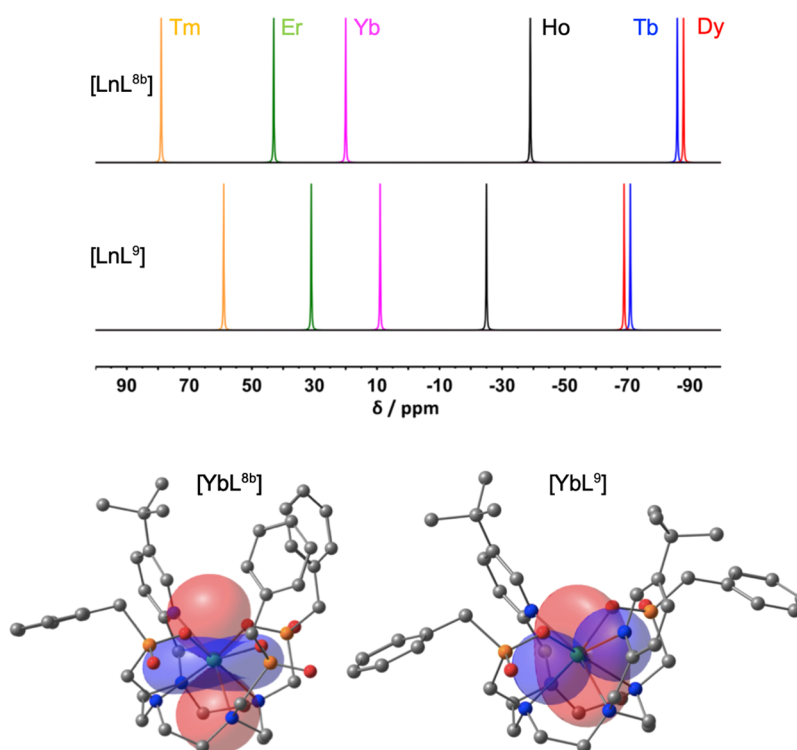


Figure 7. (top) Schematic representation of ^1Bu NMR shifts: $[\text{LnL}^{8b}]$ (upper), $[\text{LnL}^9]\text{Cl}$ (lower) (CD_3OD , 11.7 T, 295 K) (yellow, Tm; green, Er; magenta, Yb; black, Ho; red, Dy; blue, Tb). (bottom) Pseudocontact shift fields for $[\text{YbL}^{8b}]$ (left) and $[\text{YbL}^9]^+$ (right). Positive PCS, red (+200 ppm); negative, blue (−200 ppm). Twist angles of each TSAP complex were 26.4° and 18.5° , that is, greater distortion in the cationic complex.³

For $[\text{YbL}^{1b}]$, DFT was used to determine a pseudosolution structure with imposed C_3 symmetry and CASSCF-SO calculations gave the anisotropy of the susceptibility tensor (squares, Figure 8). The experimental values of $\chi_{\parallel} - \chi_{\text{av}}$ were determined assuming a fixed structural model based on experimental PCS, referenced to the diamagnetic Y(III) complex. A comparison was then made with the CASSCF-SO-calculated susceptibility anisotropy, to determine the “spectroscopic” average value of θ in solution. In $[\text{YbL}^{1b}]$, the diastereotopic methyl groups of the isopropyl substituent serve as a local probe of magnetic anisotropy. The PCS fields in acetone, water, and methanol highlight the sensitivity to solvent. The PCS field changes sign as the magnetic susceptibility anisotropy switches from “easy axis” to “easy plane” in D_2O .⁴⁶ Similar solvent dependences were found for $[\text{LnL}^{1a}]$ (Dy, Er, Eu).²

The sensitivity of magnetic anisotropy in these lanthanide complexes with small ligand field splittings was shown to have a major impact on solid-state EPR behavior.⁸⁴ The magnetic and spectroscopic properties depend upon a number of factors that cannot be disentangled: a distribution of structural parameters generates a range of B_0^2 values; an electronic structure sensitive to thermal changes of the ligand structure; thermally accessible EPR-active excited states; disordered solvation influencing the local ligand field. Each effect is present across the $[\text{LnL}^{1-3}]$ series, making interpretation of EPR spectra very difficult for systems with small magnetic anisotropy.⁸⁴

NMR SHIFT BEHAVIOR OF MOBILE LANTHANIDE TAGS ON PROTEINS

Complexes with large magnetic anisotropies are often used as tags in protein NMR to provide structural constraints,^{85,86} where large magnetic anisotropy is preferred so that PCS is measurable

even at distances of 40 Å. The tag is often attached by a flexible linker, but mobility results in big deviations from the point-dipole approximation, at <15 Å.

A generalization of McConnell’s expression, eq 4, was derived for lanthanide tag mobility in protein NMR:^{73,74,87}

$$\delta(\mathbf{r}) = -\frac{1}{3} \frac{\vec{\nabla}^T \cdot \chi_t \cdot \vec{\nabla}}{\vec{\nabla}^T \cdot \vec{\nabla}} \rho(\mathbf{r}) \quad (4)$$

where $\vec{\nabla}$ is the gradient operator, $\rho(\mathbf{r})$ is the probability distribution of the spatial position of the lanthanide tag, and subscript t indicates the traceless part of the magnetic susceptibility tensor. The susceptibility is assumed to be the same in every point of the probability density.⁷⁴ The latter assumption may be lifted, but the corresponding equation is considerably harder to solve. The partial differential eq 4 can be solved using three-dimensional Fourier transforms:⁷⁴

$$\delta(\mathbf{r}) = -\frac{1}{3} \text{Re} \left[\text{FFT}_- \left\{ \frac{\vec{k}^T \cdot \chi_t \cdot \vec{k}}{\vec{k}^T \cdot \vec{k}} \text{FFT}_+ \{ \rho(\mathbf{r}) \} \right\} \right] \quad (5)$$

where FFT_+ refers to the forward fast-Fourier transform and FFT_- the inverse. If the probability density is defined on a grid, numerical solution of eq 5 gives the PCS values. The solution of the inverse problem is possible; one can extract probability density from PCS data. Numerical solvers for both direct and inverse problems are available.⁸² The resulting lanthanide probability densities from PCS are in agreement with Double Electron–Electron Resonance (DEER) spectroscopy, and PCS fits are significantly improved near the tag (Figure 9).⁸⁷

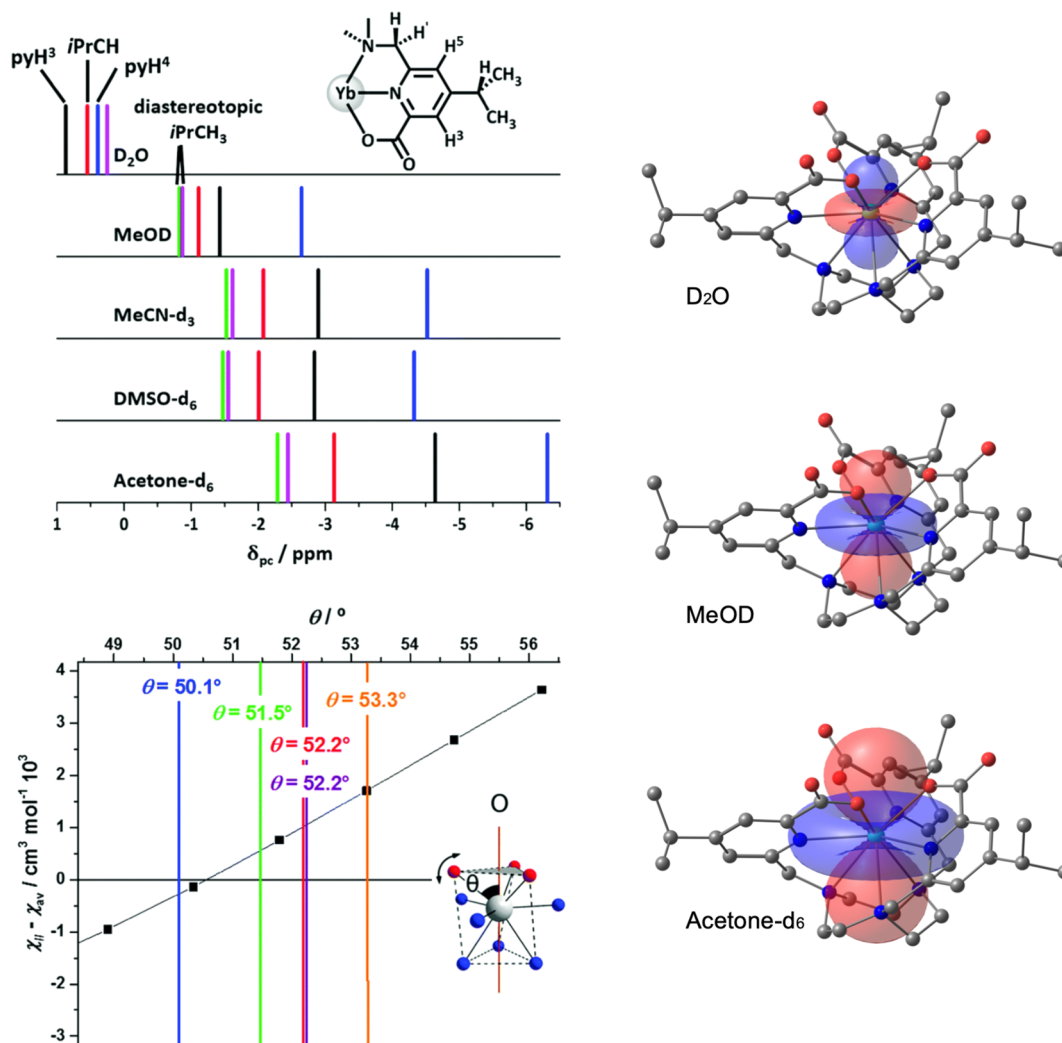


Figure 8. (left) Schematic representation of PCS (295 K, 4.7 T) for pyridyl H³, H⁵, and ⁱPr resonances of [YbL^{1b}] and variation in the susceptibility anisotropy with θ : D₂O (blue); CD₃OD (green); CD₃CN (purple); DMSO-*d*₆ (red); acetone-*d*₆ (orange); diastereotopic methyl resonances are isochronous in D₂O. (right) PCS fields for [YbL^{1b}], (using Spinach⁸²): positive PCS, red; negative, blue.⁴⁶

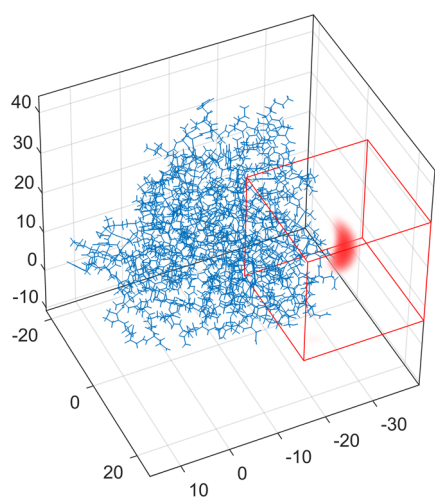


Figure 9. Tm³⁺ ion distribution (red) in a DOTA-M8 tagged S50C mutant of human carbonic anhydrase II (blue), extracted from PCS data. The red cube indicates the volume where the probability density can vary during fitting. The source code is available in Spinach;⁸² axes in Å.

LANTHANIDE RELAXATION AND ITS ANISOTROPY

Common MRI contrast agents contain magnetically isotropic Gd³⁺ ions. Their long electron relaxation times mean that PCS is absent, and the effect is only to accelerate nuclear relaxation.⁸⁸ Likewise, relaxation enhancement experiments in NMR often use magnetically isotropic Mn²⁺ or Gd³⁺ complexes to maximize the volume affected by the metal and minimize PCS.⁸⁹ Following nuclear relaxation enhancement models designed for these ions, it has often been assumed that the enhancements show a simple $1/r^6$ dependence on the electron–nuclear distance, without angular terms in the molecular frame of reference.

Nuclear relaxation enhancement by unpaired *f* electrons of lanthanide complexes has two principal components. One (“dipolar relaxation”) comes from stochastic modulation of the electron–nuclear dipolar interaction and the other (“Curie relaxation”) from rotational modulation of extra nuclear shielding caused by the presence of the unpaired electron. The angular dependence in non-Gd lanthanides⁴ was first acknowledged for Curie relaxation.⁹⁰ The reasons are twofold. First, magnetic susceptibility tensor anisotropy can be as large as the isotropic part, contradicting the assumption made by Gueron

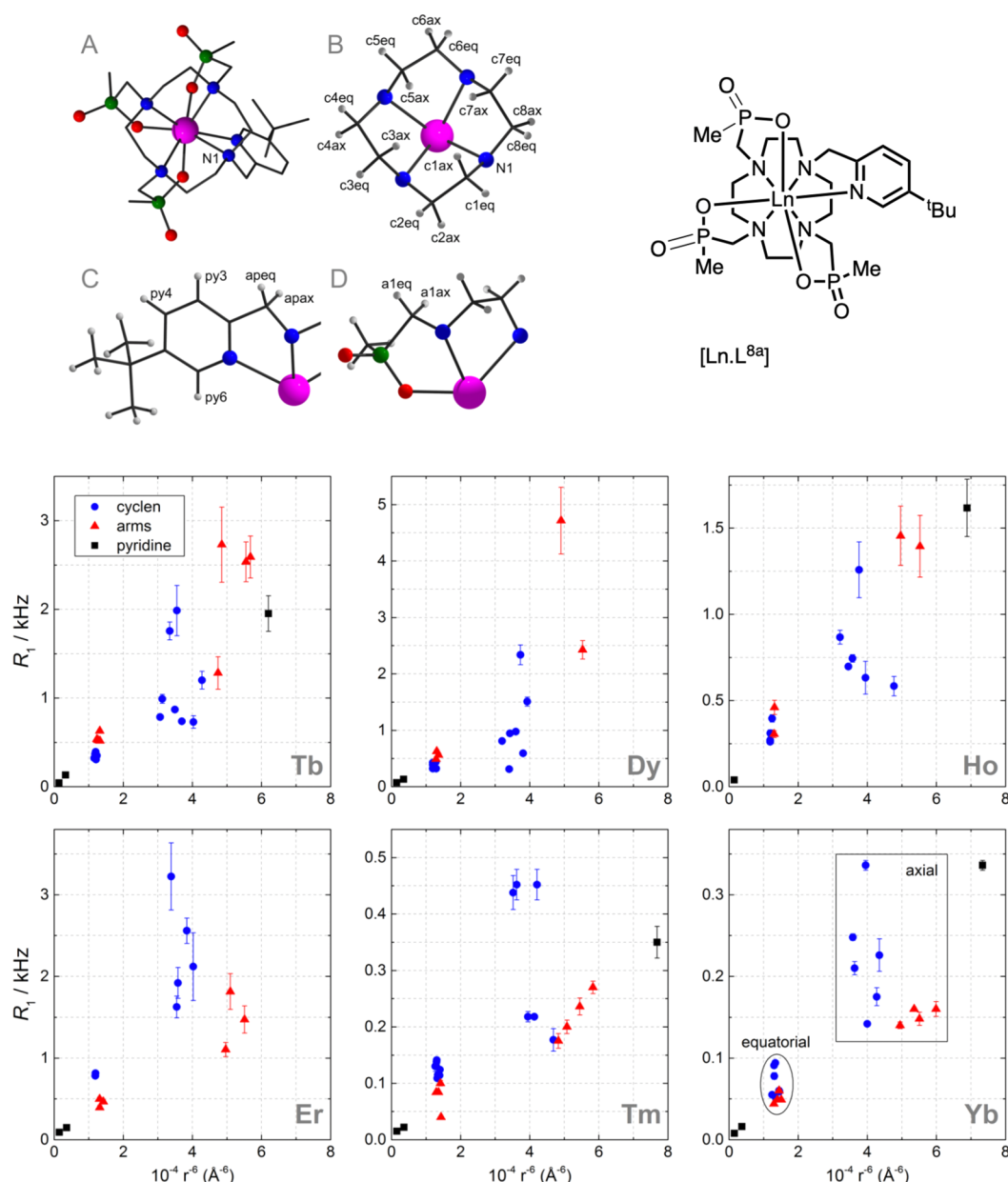


Figure 10. Longitudinal relaxation rates in $[\text{LnL}^{8a}]$ complexes as functions of Ln-H distance (r^{-6} , D_2O , 295 K, 1 T), for 12- N_4 ring protons (blue circles), ligand arms (red triangles), and pyridine protons (black squares). In the Yb set, axial and equatorial protons are indicated. A pure r^{-6} dependence is a straight line.⁴

when he derived Curie relaxation theory.⁹¹ Second, zero field splitting can be much stronger than the electron Zeeman interaction, the opposite limit from the classical Solomon–Bloembergen–Morgan theory of lanthanide-induced dipolar relaxation.⁹²

Experimental proof came from relaxation rate measurements in complexes where all nuclei in the ligand cages could be unambiguously assigned, and atomic coordinate estimates were available from DFT calculations^{28,37,38,93–95} (Chart 1 and Figure 10).

It is obvious from Figure 10 that nuclear relaxation enhancements at low magnetic field (1 T) *do not* depend simply on the distance to the lanthanide ion. The relaxation rates also appear to depend on the sign of the magnetic anisotropy: in complexes with easy-plane anisotropy (Tb, Dy, Ho), ligand arm

protons relax faster than macrocyclic ring protons; the opposite is true for the complexes with easy-axis anisotropy (Er, Tm, Yb).

Encouraged by these findings, we updated the dipolar relaxation theory⁴ to include the direction of the Ln-H vector in the molecular frame:

$$R_1^{\text{dip}} = \frac{2}{3} \left(\frac{\mu_0}{4\pi} \right)^2 \frac{\gamma_N^2}{r^6} \text{Tr}[(3\hat{r}\hat{r}^T - 1)^2 \mathbf{G}(\omega_N)]$$

$$R_2^{\text{dip}} = \frac{1}{3} \left(\frac{\mu_0}{4\pi} \right)^2 \frac{\gamma_N^2}{r^6} \text{Tr}[(3\hat{r}\hat{r}^T - 1)^2 (\mathbf{G}(0) + \mathbf{G}(\omega_N))]$$
(6)

$$\mathbf{G}(\omega) = \int_0^\infty \mathbf{G}(\tau) e^{-\tau/\tau_R} e^{-i\omega\tau} d\tau$$
(7)

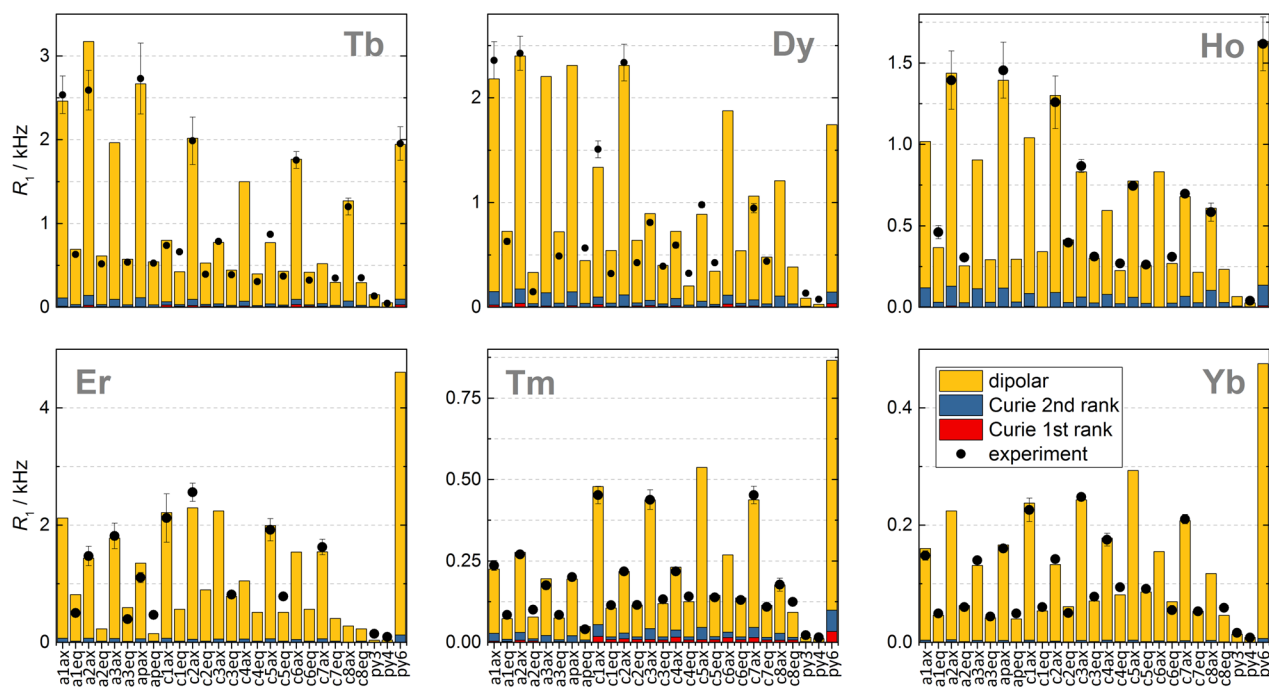


Figure 11. Experimental longitudinal relaxation rates (black dots) for the ligand cage nuclei of $[\text{LnL}^{8a}]$ in D_2O at 295 K and 1 T. The calculated rates are shown as bars and color-coded by the mechanism.⁴

where the spectral power density $G(\omega)$ is no longer a scalar but a tensor accommodating stochastic dynamics of the electron spin as well as molecular accommodating stochastic dynamics of the electron spin as well as molecular rotation, and \hat{r} is the unit vector pointing in the same direction as \vec{r} ; further details may be found in the paper cited above.

Similar observations were made at higher field 9.4 T for $[\text{LnL}^{8a}]$ complexes ($\text{Ln} = \text{Tb}–\text{Yb}$), where the Curie contribution dominates. For Curie relaxation, it turned out to be essential to account for the antisymmetric component in the total nuclear shielding tensor

$$\sigma = \sigma_0 - \mathbf{D} \cdot \chi \quad (8)$$

that includes diamagnetic shielding tensor σ_0 and paramagnetic shielding tensor, which is proportional to the dipolar matrix \mathbf{D} and magnetic susceptibility tensor χ . This is necessary because the antisymmetric part is significant here; the product of two symmetric matrices is only symmetric when they commute. With the relevant extra terms in place, the Curie relaxation rates become

$$\begin{aligned} R_1^{\text{Curie+CSA}} &= \frac{1}{2} \Lambda_\sigma^2 \omega_N^2 \frac{\tau_R}{1 + 9\omega_N^2 \tau_R^2} \\ &+ \frac{2}{15} \Delta_\sigma^2 \omega_N^2 \frac{\tau_R}{1 + \omega_N^2 \tau_R^2} \\ R_2^{\text{Curie+CSA}} &= \frac{1}{4} \Lambda_\sigma^2 \omega_N^2 \frac{\tau_R}{1 + 9\omega_N^2 \tau_R^2} \\ &+ \frac{1}{45} \Delta_\sigma^2 \omega_N^2 \left(4\tau_R + \frac{3\tau_R}{1 + \omega_N^2 \tau_R^2} \right) \end{aligned} \quad (9)$$

$$\begin{aligned} \Lambda_\sigma^2 &= (\sigma_{XY} - \sigma_{YX})^2 + (\sigma_{XZ} - \sigma_{ZX})^2 + (\sigma_{YZ} - \sigma_{ZY})^2 \\ \Delta_\sigma^2 &= \sigma_{XX}^2 + \sigma_{YY}^2 + \sigma_{ZZ}^2 - \sigma_{XX}\sigma_{YY} - \sigma_{XX}\sigma_{ZZ} \\ &- \sigma_{YY}\sigma_{ZZ} + \frac{3}{4}[(\sigma_{XY} + \sigma_{YX})^2 + (\sigma_{XZ} + \sigma_{ZX})^2 \\ &+ (\sigma_{YZ} + \sigma_{ZY})^2] \end{aligned} \quad (10)$$

here, Λ_σ^2 is the first and Δ_σ^2 the second rank invariant of the chemical shielding tensor. These equations have been incorporated into Spinach;⁸² for $[\text{LnL}^{8a}]$, the modifications yielded a much better agreement with experiment (Figure 11).⁴

In summary, the presence of magnetic anisotropy required a fundamental update of the relevant nuclear relaxation theories. These updates revealed strong molecular-frame angular dependencies in paramagnetic relaxation enhancements. In systems with large magnetic anisotropy and at short electron–nuclear distances, the classical Solomon–Bloembergen–Morgan and Gueron expressions should not be used.

SUMMARY AND CONCLUSIONS

The ligand field for a lanthanide complex varies with the nature of the ligand, metal ion, and its environment. The size and sign of ligand field parameters are difficult to determine experimentally, but information can be gained using optical spectroscopy with Eu(III) complexes.⁹ They are sensitive to several factors including the nature and polarizability of the overall ligand and donor atoms, the type and degree of geometric distortion, the extent of solvent dipolar interactions, and specific hydrogen bonding effects and the degree of supramolecular order.

Bleaney's magnetic anisotropy theory provided guidance in rationalizing NMR PCS data. However, its crude approximations and limitations are apparent. In explaining the nature and magnitude of PCS data, both the ligand field splitting and the type, size, and orientation of the principal component of the magnetic susceptibility tensor are key. The latter can be determined by careful magneto-structural correlations^{27,31,2,46}

assessed by VT magnetic susceptibility measurements, low temperature EPR studies, and modern computational methods.

Considerable caution is needed using PCS data for structural refinement. Such methods are used in biomolecular analyses but may fail when the lanthanide ion is permuted. Delving more deeply, the ordering, nature, and relative Boltzmann population of the m_J sublevels for a given lanthanide ion complex is key to understanding the overall magnetic susceptibility and its directional dependences.

The nuclear relaxation induced by lanthanide ions can be anisotropic in the molecular frame, and accounting for this anisotropy can drastically improve agreement between experiment and theoretical models. Analyses based only on distance variations are a crude approximation for both dipolar and Curie relaxation mechanisms. Biomolecular structural refinement using lanthanide spin tags must account for this anisotropy or risk significant errors; any work using simple $1/r^6$ models for lanthanide labeled systems should be considered with appropriate caution.

AUTHOR INFORMATION

Corresponding Author

David Parker – Department of Chemistry, Durham University, Durham DH1 3LE, U.K.; orcid.org/0000-0001-5281-5146; Email: david.parker@dur.ac.uk

Authors

Elizaveta A. Suturina – Department of Chemistry, University of Bath, Bath BA2 7AY, U.K.

Ilya Kuprov – School of Chemistry, University of Southampton, Southampton SO17 1BJ, U.K.; orcid.org/0000-0003-0430-2682

Nicholas F. Chilton – Department of Chemistry, School of Natural Sciences, The University of Manchester, Manchester M13 9PL, U.K.; orcid.org/0000-0002-8604-0171

Complete contact information is available at:

<https://pubs.acs.org/10.1021/acs.accounts.0c00275>

Author Contributions

The manuscript was written through contributions of all authors. All authors have given approval to the final version of the manuscript.

Notes

The authors declare no competing financial interest.

Biographies

David Parker was born in Leadgate, England, on 30th July 1956. Educated in the state sector, he read Chemistry at Oxford University (1974–1978) and remained there to study with John Brown for a DPhil, which he gained in 1980. Following a NATO Fellowship in Strasbourg with Jean-Marie Lehn, he returned to the NE of England in early 1982 as a Lecturer in Chemistry at Durham University. He gained several national and international awards and prizes for work that embraces several aspects of contemporary chemistry, including the design of sensors, targeted imaging probes, and therapeutic agents, as well as major contributions to chiral analysis and mechanistic studies. He is a Professor of Chemistry at Durham University.

Elizaveta Suturina studied physics at Novosibirsk State University where she obtained her undergraduate degree and DPhil in chemical physics working in the group of Nina Gritsan. She then moved to work in Max-Planck Institute with Frank Neese and Mihail Atanasov on ab

initio modeling of molecular magnetic properties and then joined Ilya Kuprov's group to work on NMR theory and modelling of paramagnetic systems. In 2018, she was awarded the Prize fellowship from the University of Bath where she is currently establishing her research group.

Ilya Kuprov is a magnetic resonance specialist and the leading author of Spinach, an advanced spin dynamics simulation package. He did his undergraduate degrees at Novosibirsk State University before moving to Oxford for a DPhil. He was a Lecturer at Durham University and is presently an Associate Professor at Southampton. He is the Secretary of the Electron Spin Resonance Group of the Royal Society of Chemistry and an Associate Editor at *Science Advances*. He has published about a hundred papers, principally on the theoretical and computational aspects of magnetic resonance spectroscopy and imaging.

Nicholas Chilton obtained his B.Sc. Adv. (Hons.) in chemistry in the group of Prof. Keith Murray at Monash University, Australia, before moving to the UK in 2013 to undertake his Ph.D. with Profs. Richard Winpenny and Eric McInnes at The University of Manchester. In 2016, he obtained a Ramsay Memorial Research Fellowship and started his own research group at The University of Manchester, followed by a Presidential Fellowship in 2018 and a Royal Society University Research Fellowship in 2019. He is currently a Senior Lecturer at The University of Manchester and holds a number of prizes and awards.

ACKNOWLEDGMENTS

We thank EPSRC for grant support (EP/N007034/1, EP/N006909/1, EP/N006895/1) and talented colleagues in Manchester, Southampton, Bath, and Durham whose names appear in the reference list for their conscientiousness, resilience, and excellence.

REFERENCES

- (1) Suturina, E. A.; Mason, K.; Gerdal, C. F.; Kuprov, I.; Parker, D. Beyond Bleaney's Theory: Experimental and Theoretical Analysis of Periodic Trends in Lanthanide-Induced Chemical Shift. *Angew. Chem., Int. Ed.* **2017**, *56*, 12215–12218.
- (2) Vonci, M.; Mason, K.; Suturina, E. A.; Frawley, A. T.; Worswick, S. G.; Kuprov, I.; Parker, D.; McInnes, E. J.; Chilton, N. F. Rationalization of Anomalous Pseudocontact Shifts and Their Solvent Dependence in a Series of C_3 -Symmetric Lanthanide Complexes. *J. Am. Chem. Soc.* **2017**, *139*, 14166–14172.
- (3) Harnden, A. C.; Suturina, E. A.; Batsanov, A. S.; Senanayake, P. K.; Fox, M. A.; Mason, K.; Vonci, M.; McInnes, E. J.; Chilton, N. F.; Parker, D. Unravelling the Complexities of Pseudocontact Shift Analysis in Lanthanide Coordination Complexes of Differing Symmetry. *Angew. Chem.* **2019**, *131*, 10396–10400.
- (4) Suturina, E. A.; Mason, K.; Gerdal, C. F.; Chilton, N. F.; Parker, D.; Kuprov, I. Lanthanide-induced relaxation anisotropy. *Phys. Chem. Chem. Phys.* **2018**, *20*, 17676–17686.
- (5) Stevens, K. Matrix elements and operator equivalents connected with the magnetic properties of rare earth ions. *Proc. Phys. Soc., London, Sect. A* **1952**, *65*, 209.
- (6) Stevens, K. W. H. Matrix Elements and Operator Equivalents Connected with the Magnetic Properties of Rare Earth Ions. *Proc. Phys. Soc., London, Sect. A* **1952**, *65*, 209–215.
- (7) Mulak, J.; Gajek, Z. *The Effective Crystal Field Potential*; Elsevier, 2000.
- (8) Eyring, L.; Gschneidner, K. A.; Lander, G. H. *Handbook on the Physics and Chemistry of Rare Earths*; Elsevier, 2002; Vol. 32.
- (9) Wybourne, B. G.; Smentek, L. *Optical Spectroscopy of Lanthanides: Magnetic and Hyperfine Interactions*; CRC Press, 2007.
- (10) Bünzli, J.-C. G.; Eliseeva, S. V. Basics of Lanthanide Photophysics. In *Lanthanide Luminescence: Photophysical, Analytical and Biological Aspects*; Hänninen, P., Härmä, H., Eds.; Springer Berlin Heidelberg: Berlin, Heidelberg, 2011; pp 1–45.

- (11) Bleaney, B. Nuclear magnetic resonance shifts in solution due to lanthanide ions. *J. Magn. Reson. (1969-1992)* **1972**, *8*, 91–100.
- (12) Binnemans, K.; Görller-Walrand, C. A simple model for crystal field splittings of the 7F1 and 5D1 energy levels of Eu3+. *Chem. Phys. Lett.* **1995**, *245*, 75–78.
- (13) Finney, K. L. N.; Harnden, A. C.; Rogers, N. J.; Senanayake, P. K.; Blamire, A. M.; O'Hogain, D.; Parker, D. Simultaneous triple imaging with two PARASHIFT probes: encoding anatomical, pH and temperature information using magnetic resonance shift imaging. *Chem. - Eur. J.* **2017**, *23*, 7976–7989.
- (14) Binnemans, K. Interpretation of europium(III) spectra. *Coord. Chem. Rev.* **2015**, *295*, 1–45.
- (15) Ungur, L.; Chibotaru, L. F. Ab Initio Crystal Field for Lanthanides. *Chem. - Eur. J.* **2017**, *23*, 3708–3718.
- (16) Görller-Walrand, C.; Binnemans, K. Chapter 155 Rationalization of crystal-field parametrization. In *Handbook on the Physics and Chemistry of Rare Earths*; Elsevier **1996**, *23*, 121–283.
- (17) Senanayake, P. K.; Rogers, N. J.; Finney, K. L. N.; Harvey, P.; Funk, A. M.; Wilson, J. I.; O'Hogain, D.; Maxwell, R.; Parker, D.; Blamire, A. M. A new paramagnetically shifted imaging probe for MRI. *Magn. Reson. Med.* **2017**, *77*, 1307–1317.
- (18) Harnden, A. C.; Parker, D.; Rogers, N. J. Employing paramagnetic shift for responsive MRI probes. *Coord. Chem. Rev.* **2019**, *383*, 30–42.
- (19) Liu, J.; Reta, D.; Cleghorn, J. A.; Yeoh, Y. X.; Ortu, F.; Goodwin, C. A.; Chilton, N. F.; Mills, D. P. Light Lanthanide Metalloccenium Cations Exhibiting Weak Equatorial Anion Interactions. *Chem. - Eur. J.* **2019**, *25*, 7749–7758.
- (20) Ma, C.-G.; Brik, M.; Kiisk, V.; Kangur, T.; Sildos, I. Spectroscopic and crystal-field analysis of energy levels of Eu3+ in SnO2 in comparison with ZrO2 and TiO2. *J. Alloys Compd.* **2011**, *509*, 3441–3451.
- (21) Auzel, F.; Malta, O. A scalar crystal field strength parameter for rare-earth ions: meaning and usefulness. *J. Phys. (Paris)* **1983**, *44*, 201–206.
- (22) Malta, O.; Antic-Fidancev, E.; Lemaitre-Blaise, M.; Milicic-Tang, A.; Taibi, M. The crystal field strength parameter and the maximum splitting of the 7F1 manifold of the Eu3+ ion in oxides. *J. Alloys Compd.* **1995**, *228*, 41–44.
- (23) Gendron, F.; Moore, B., II; Cador, O.; Pointillart, F.; Autschbach, J.; Le Guennic, B. Ab Initio Study of Circular Dichroism and Circularly Polarized Luminescence of Spin-Allowed and Spin-Forbidden Transitions: From Organic Ketones to Lanthanide Complexes. *J. Chem. Theory Comput.* **2019**, *15*, 4140–4155.
- (24) Souza, A.; Dos Santos, M. C. The J-mixing effect in Ln3+ ions crystal field levels. *Chem. Phys. Lett.* **2012**, *521*, 138–141.
- (25) Jensen, J.; Mackintosh, A. R. *Rare Earth Magnetism*; Clarendon Press Oxford, 1991.
- (26) Kurzen, H.; Bovigny, L.; Bulloni, C.; Daul, C. Electronic structure and magnetic properties of lanthanide 3+ cations. *Chem. Phys. Lett.* **2013**, *574*, 129–132.
- (27) Hölsä, J.; Lastusaari, M.; Niittykoski, J.; Puche, R. S. Interplay between crystal structure and magnetic susceptibility of tetragonal ROBr. *Phys. Chem. Chem. Phys.* **2002**, *4*, 3091–3097.
- (28) Butler, S. J.; Delbianco, M.; Lamarque, L.; McMahon, B. K.; Neil, E. R.; Pal, R.; Parker, D.; Walton, J. W.; Zwier, J. M. EuroTracker® dyes: design, synthesis, structure and photophysical properties of very bright europium complexes and their use in bioassays and cellular optical imaging. *Dalton Transactions* **2015**, *44*, 4791–4803.
- (29) Delbianco, M.; Sadovnikova, V.; Bourrier, E.; Mathis, G.; Lamarque, L.; Zwier, J. M.; Parker, D. Bright, Highly Water-Soluble Triazacyclononane Europium Complexes To Detect Ligand Binding with Time-Resolved FRET Microscopy. *Angew. Chem., Int. Ed.* **2014**, *53*, 10718–10722.
- (30) Shuvaev, S.; Starck, M.; Parker, D. Responsive, Water-Soluble Europium (III) Luminescent Probes. *Chem. - Eur. J.* **2017**, *23*, 9974–9989.
- (31) Blackburn, O. A.; Edkins, R. M.; Faulkner, S.; Kenwright, A. M.; Parker, D.; Rogers, N. J.; Shuvaev, S. Electromagnetic susceptibility anisotropy and its importance for paramagnetic NMR and optical spectroscopy in lanthanide coordination chemistry. *Dalton Transactions* **2016**, *45*, 6782–6800.
- (32) Ofelt, G. Intensities of crystal spectra of rare-earth ions. *J. Chem. Phys.* **1962**, *37*, 511–520.
- (33) Judd, B. R. Optical absorption intensities of rare-earth ions. *Phys. Rev.* **1962**, *127*, 750.
- (34) Jørgensen, C. K.; Judd, B. Hypersensitive pseudoquadrupole transitions in lanthanides. *Mol. Phys.* **1964**, *8*, 281–290.
- (35) Piguet, C.; Gherghel, C. F. Paramagnetic NMR lanthanide induced shifts for extracting solution structures. *Handbook on the Physics and Chemistry of Rare Earths* **2003**, *33*, 353–463.
- (36) Bertini, I.; Luchinat, C.; Parigi, G. Magnetic susceptibility in paramagnetic NMR. *Prog. Nucl. Magn. Reson. Spectrosc.* **2002**, *40*, 249.
- (37) Funk, A. M.; Finney, K. L. N.; Harvey, P.; Kenwright, A. M.; Neil, E. R.; Rogers, N. J.; Senanayake, P. K.; Parker, D. Critical analysis of the limitations of Bleaney's theory of magnetic anisotropy in paramagnetic lanthanide coordination complexes. *Chemical Science* **2015**, *6*, 1655–1662.
- (38) Castro, G.; Regueiro-Figueroa, M.; Esteban-Gómez, D.; Pérez-Lourido, P.; Platas-Iglesias, C.; Valencia, L. Magnetic anisotropies in rhombic lanthanide (III) complexes do not conform to Bleaney's theory. *Inorg. Chem.* **2016**, *55*, 3490–3497.
- (39) Suturina, E. A.; Mason, K.; Botta, M.; Carniato, F.; Kuprov, I.; Chilton, N. F.; McInnes, E. J.; Vonci, M.; Parker, D. Periodic trends and hidden dynamics of magnetic properties in three series of triazacyclononane lanthanide complexes. *Dalton Transactions* **2019**, *48*, 8400–8409.
- (40) Beeby, A.; Clarkson, I. M.; Dickins, R. S.; Faulkner, S.; Parker, D.; Royle, L.; de Sousa, A. S.; Williams, J. A. G.; Woods, M. Non-radiative deactivation of the excited states of europium, terbium and ytterbium complexes by proximate energy-matched OH, NH and CH oscillators: an improved luminescence method for establishing solution hydration states. *J. Chem. Soc., Perkin Trans. 2* **1999**, *2*, 493–504.
- (41) Aime, S.; Botta, M.; Parker, D.; Williams, J. G. Extent of hydration of octadentate lanthanide complexes incorporating phosphinate donors: Solution relaxometry and luminescence studies. *J. Chem. Soc., Dalton Trans.* **1996**, 17–23.
- (42) Woods, M.; Aime, S.; Botta, M.; Howard, J. A.; Moloney, J. M.; Navet, M.; Parker, D.; Port, M.; Rousseaux, O. Correlation of water exchange rate with isomeric composition in diastereoisomeric gadolinium complexes of tetra (carboxyethyl) dota and related macrocyclic ligands. *J. Am. Chem. Soc.* **2000**, *122*, 9781–9792.
- (43) Kotek, J.; Rudovský, J.; Hermann, P.; Lukeš, I. Three in One: TSA, TSA', and SA Units in One Crystal Structure of a Yttrium (III) Complex with a Monophosphinated H4dota Analogue. *Inorg. Chem.* **2006**, *45*, 3097–3102.
- (44) Dickins, R. S.; Parker, D.; Bruce, J. I.; Tozer, D. J. Correlation of optical and NMR spectral information with coordination variation for axially symmetric macrocyclic Eu (III) and Yb (III) complexes: axial donor polarisability determines ligand field and cation donor preference. *Dalton Transactions* **2003**, 1264–1271.
- (45) Bari, L. D.; Pintacuda, G.; Salvadori, P.; Dickins, R. S.; Parker, D. Effect of axial ligation on the magnetic and electronic properties of lanthanide complexes of octadentate ligands. *J. Am. Chem. Soc.* **2000**, *122*, 9257–9264.
- (46) Mason, K.; Harnden, A. C.; Patrick, C. W.; Poh, A. W.; Batsanov, A. S.; Suturina, E. A.; Vonci, M.; McInnes, E. J.; Chilton, N. F.; Parker, D. Exquisite sensitivity of the ligand field to solvation and donor polarisability in coordinatively saturated lanthanide complexes. *Chem. Commun.* **2018**, *54*, 8486–8489.
- (47) Richardson, F. S. On the calculation of electric dipole strengths of 4f→4f transitions in lanthanide complexes. *Chem. Phys. Lett.* **1982**, *86*, 47–50.
- (48) Kuroda, R.; Mason, S. F.; Rosini, C. Crystal structure and single-crystal spectra of Gd (Eu) Al3 (BO3)4. Anisotropic ligand polarization contributions to the f-f transition probabilities in Eu III. *J. Chem. Soc., Faraday Trans. 2* **1981**, *77*, 2125–2140.

- (49) Lowe, M. P.; Parker, D.; Reany, O.; Aime, S.; Botta, M.; Castellano, G.; Gianolio, E.; Pagliarin, R. pH-dependent modulation of relaxivity and luminescence in macrocyclic gadolinium and europium complexes based on reversible intramolecular sulfonamide ligation. *J. Am. Chem. Soc.* **2001**, *123*, 7601–7609.
- (50) Krchová, T.; Herynek, V.; Gálisová, A.; Blahut, J.; Hermann, P.; Kotek, J. Eu (III) Complex with DO3A-amino-phosphonate Ligand as a Concentration-Independent pH-Responsive Contrast Agent for Magnetic Resonance Spectroscopy (MRS). *Inorg. Chem.* **2017**, *56*, 2078–2091.
- (51) Shuvaev, S.; Suturina, E. A.; Mason, K.; Parker, D. Chiral probes for α -1-AGP reporting by species-specific induced circularly polarised luminescence. *Chemical Science* **2018**, *9*, 2996–3003.
- (52) Rinehart, J. D.; Long, J. R. Exploiting single-ion anisotropy in the design of f-element single-molecule magnets. *Chemical Science* **2011**, *2*, 2078–2085.
- (53) Sievers, J. Asphericity of 4f-shells in their Hund's rule ground states. *Z. Phys. B: Condens. Matter Quanta* **1982**, *45*, 289–296.
- (54) Chilton, N. F.; Collison, D.; McInnes, E. J.; Winpenny, R. E.; Soncini, A. An electrostatic model for the determination of magnetic anisotropy in dysprosium complexes. *Nat. Commun.* **2013**, *4*, 2551.
- (55) Sorace, L.; Benelli, C.; Gatteschi, D. Lanthanides in molecular magnetism: old tools in a new field. *Chem. Soc. Rev.* **2011**, *40*, 3092–3104.
- (56) Mironov, V. S.; Galyametdinov, Y. G.; Ceulemans, A.; Görlner-Walrand, C.; Binnemans, K. Room-temperature magnetic anisotropy of lanthanide complexes: A model study for various coordination polyhedra. *J. Chem. Phys.* **2002**, *116*, 4673–4685.
- (57) Dai, L.; Zhang, J.; Chen, Y.; Mackenzie, L. E.; Pal, R.; Law, G.-L. Synthesis of Water-Soluble Chiral DOTA Lanthanide Complexes with Predominantly Twisted Square Antiprism Isomers and Circularly Polarized Luminescence. *Inorg. Chem.* **2019**, *58*, 12506–12510.
- (58) Woods, M.; Payne, K. M.; Valente, E. J.; Kucera, B. E.; Young, V. G., Jr Crystal structures of DOTMA chelates from Ce³⁺ to Yb³⁺: evidence for a continuum of metal ion hydration states. *Chem. - Eur. J.* **2019**, *25*, 9997–10005.
- (59) Mason, S. F.; Peacock, R. D.; Stewart, B. Ligand-polarization contributions to the intensity of hypersensitive trivalent lanthanide transitions. *Mol. Phys.* **1975**, *30*, 1829–1841.
- (60) Mason, S. F. The ligand polarization model for the spectra of metal complexes: The dynamic coupling transition probabilities. In *Electrons and Transitions*; Springer, 1980; pp 43–81.
- (61) Reid, M. F.; Richardson, F. S. Anisotropic ligand polarizability contributions to lanthanide 4f → 4f intensity parameters. *Chem. Phys. Lett.* **1983**, *95*, 501–506.
- (62) Poh, A. W.; Aguilar, J. A.; Kenwright, A. M.; Mason, K.; Parker, D. Aggregation of Rare Earth Coordination Complexes in Solution Studied by Paramagnetic and DOSY NMR. *Chem. - Eur. J.* **2018**, *24*, 16170–16175.
- (63) McConnell, H. M. Theory of nuclear magnetic shielding in molecules. I. Long-range dipolar shielding of protons. *J. Chem. Phys.* **1957**, *27*, 226–229.
- (64) Peters, J.; Huskens, J.; Raber, D. Lanthanide induced shifts and relaxation rate enhancements. *Prog. Nucl. Magn. Reson. Spectrosc.* **1996**, *28*, 283–350.
- (65) Mironov, V. S.; Galyametdinov, Y. G.; Ceulemans, A.; Görlner-Walrand, C.; Binnemans, K. Influence of crystal-field perturbations on the room-temperature magnetic anisotropy of lanthanide complexes. *Chem. Phys. Lett.* **2001**, *345*, 132–140.
- (66) McGarvey, B. R. Temperature dependence of the pseudocontact shift in lanthanide shift reagents. *J. Magn. Reson. (1969-1992)* **1979**, *33*, 445–455.
- (67) Boulon, M. E.; Cucinotta, G.; Luzon, J.; Degl'Innocenti, C.; Perfetti, M.; Bernot, K.; Calvez, G.; Caneschi, A.; Sessoli, R. Magnetic anisotropy and spin-parity effect along the series of lanthanide complexes with DOTA. *Angew. Chem., Int. Ed.* **2013**, *52*, 350–354.
- (68) Cucinotta, G.; Perfetti, M.; Luzon, J.; Etienne, M.; Car, P. E.; Caneschi, A.; Calvez, G.; Bernot, K.; Sessoli, R. Magnetic anisotropy in a dysprosium/DOTA single-molecule magnet: beyond simple magneto-structural correlations. *Angew. Chem., Int. Ed.* **2012**, *51*, 1606–1610.
- (69) Briganti, M.; Garcia, G. F.; Jung, J.; Sessoli, R.; Le Guennic, B.; Totti, F. Covalency and magnetic anisotropy in lanthanide single molecule magnets: the DyDOTA archetype. *Chemical Science* **2019**, *10*, 7233–7245.
- (70) Jung, J.; Islam, M. A.; Pecoraro, V. L.; Mallah, T.; Berthon, C.; Bolvin, H. Derivation of lanthanide series crystal field parameters from first principles. *Chem. - Eur. J.* **2019**, *25*, 15112–15122.
- (71) Ungur, L.; Chibotaru, L. F. Ab initio crystal field for lanthanides. *Chem. - Eur. J.* **2017**, *23*, 3708–3718.
- (72) Golding, R.; Pykkö, P. On the theory of pseudocontact NMR shifts due to lanthanide complexes. *Mol. Phys.* **1973**, *26*, 1389–1396.
- (73) Charnock, G.; Kuprov, I. A partial differential equation for pseudocontact shift. *Phys. Chem. Chem. Phys.* **2014**, *16*, 20184–20189.
- (74) Suturina, E. A.; Kuprov, I. Pseudocontact shifts from mobile spin labels. *Phys. Chem. Chem. Phys.* **2016**, *18*, 26412–26422.
- (75) Golding, R.; Halton, M. A theoretical study of the ¹⁴N and ¹⁷O N.M.R. shifts in lanthanide complexes. *Aust. J. Chem.* **1972**, *25*, 2577–2581.
- (76) Reilley, C. N.; Good, B. W.; Allendoerfer, R. D. Separation of contact and dipolar lanthanide induced nuclear magnetic resonance shifts: evaluation and application of some structure independent methods. *Anal. Chem.* **1976**, *48*, 1446–1458.
- (77) Kreidt, E.; Bischof, C.; Platas-Iglesias, C.; Seitz, M. Magnetic Anisotropy in Functionalized Bipyridyl Cryptates. *Inorg. Chem.* **2016**, *55*, 5549–5557.
- (78) Esteban-Gómez, D.; Büldt, L. A.; Pérez-Lourido, P.; Valencia, L.; Seitz, M.; Platas-Iglesias, C. Understanding the Optical and Magnetic Properties of Ytterbium (III) Complexes. *Inorg. Chem.* **2019**, *58*, 3732–3743.
- (79) Parigi, G.; Benda, L.; Ravera, E.; Romanelli, M.; Luchinat, C. Pseudocontact shifts and paramagnetic susceptibility in semiempirical and quantum chemistry theories. *J. Chem. Phys.* **2019**, *150*, 144101.
- (80) Benda, L.; Mareš, J.; Ravera, E.; Parigi, G.; Luchinat, C.; Kaupp, M.; Vaara, J. Pseudo-Contact NMR Shifts over the Paramagnetic Metalloprotein CoMMP-12 from First Principles. *Angew. Chem., Int. Ed.* **2016**, *55*, 14713–14717.
- (81) Benda, L.; Mareš, J.; Ravera, E.; Parigi, G.; Luchinat, C.; Kaupp, M.; Vaara, J. Pseudo-Contact NMR Shifts over the Paramagnetic Metalloprotein CoMMP-12 from First Principles. *Angew. Chem.* **2016**, *128*, 14933–14937.
- (82) Hogben, H.; Krzystyniak, M.; Charnock, G.; Hore, P.; Kuprov, I. Spinach—a software library for simulation of spin dynamics in large spin systems. *J. Magn. Reson.* **2011**, *208*, 179–194.
- (83) Mason, K.; Rogers, N. J.; Suturina, E. A.; Kuprov, I.; Aguilar, J. A.; Batsanov, A. S.; Yufit, D. S.; Parker, D. PARASHIFT probes: solution NMR and X-ray structural studies of macrocyclic ytterbium and yttrium complexes. *Inorg. Chem.* **2017**, *56*, 4028–4038.
- (84) Vonci, M.; Mason, K.; Neil, E. R.; Yufit, D. S.; McInnes, E. J.; Parker, D.; Chilton, N. F. Sensitivity of Magnetic Anisotropy in the Solid State for Lanthanide Complexes with Small Crystal Field Splitting. *Inorg. Chem.* **2019**, *58*, 5733–5745.
- (85) Bertini, I.; Luchinat, C.; Parigi, G.; Pierattelli, R. NMR spectroscopy of paramagnetic metalloproteins. *ChemBioChem* **2005**, *6*, 1536–1549.
- (86) Otting, G. Protein NMR using paramagnetic ions. *Annu. Rev. Biophys.* **2010**, *39*, 387–405.
- (87) Suturina, E. A.; Häussinger, D.; Zimmermann, K.; Garbuio, L.; Yulikov, M.; Jeschke, G.; Kuprov, I. Model-free extraction of spin label position distributions from pseudocontact shift data. *Chemical science* **2017**, *8*, 2751–2757.
- (88) Caravan, P. Protein-targeted gadolinium-based magnetic resonance imaging (MRI) contrast agents: design and mechanism of action. *Acc. Chem. Res.* **2009**, *42*, 851–862.
- (89) Clore, G. M.; Iwahara, J. Theory, practice, and applications of paramagnetic relaxation enhancement for the characterization of transient low-population states of biological macromolecules and their complexes. *Chem. Rev.* **2009**, *109*, 4108–4139.

(90) Vega, A. J.; Fiat, D. Nuclear relaxation processes of paramagnetic complexes the slow-motion case. *Mol. Phys.* **1976**, *31*, 347–355.

(91) Guéron, M. Nuclear relaxation in macromolecules by paramagnetic ions: a novel mechanism. *J. Magn. Reson. (1969-1992)* **1975**, *19*, 58–66.

(92) Bloembergen, N. Proton relaxation times in paramagnetic solutions. *J. Chem. Phys.* **1957**, *27*, 572–573.

(93) Funk, A. M.; Harvey, P.; Finney, K.-L. N.; Fox, M. A.; Kenwright, A. M.; Rogers, N. J.; Senanayake, P. K.; Parker, D. Challenging lanthanide relaxation theory: erbium and thulium complexes that show NMR relaxation rates faster than dysprosium and terbium analogues. *Phys. Chem. Chem. Phys.* **2015**, *17*, 16507–16511.

(94) Rogers, N. J.; Finney, K.-L. N.; Senanayake, P. K.; Parker, D. Another challenge to paramagnetic relaxation theory: a study of paramagnetic proton NMR relaxation in closely related series of pyridine-derivatised dysprosium complexes. *Phys. Chem. Chem. Phys.* **2016**, *18*, 4370–4375.

(95) Funk, A. M.; Fries, P. H.; Harvey, P.; Kenwright, A. M.; Parker, D. Experimental measurement and theoretical assessment of fast lanthanide electronic relaxation in solution with four series of isostructural complexes. *J. Phys. Chem. A* **2013**, *117*, 905–917.